Perturbations in the surface structure of A22 Iraq foot-and-mouth disease virus accompanying coupled changes in host cell specificity and antigenicity

Stephen Curry[1†], Elizabeth Fry[2], Wendy Blakemore[1], Robin Abu-Ghazaleh[1], Terry Jackson[1], Andrew King[1], Susan Lea[2], John Newman[1], David Rowlands[3] and David Stuart[2,4*]

Background: Foot-and-mouth disease virus (FMDV) is an extremely infectious and antigenically diverse picornavirus of cloven-hoofed animals. Strains of the A22 subtype have been reported to change antigenically when adapted to different growth conditions. To investigate the structural basis of this phenomenon we have determined the structures of two variants of an A22 virus.

Results: The structures of monolayer- and suspension-cell-adapted A22 FMDV have been determined by X-ray crystallography. Picornaviruses comprise four capsid proteins, VP1–4. The major antigenic loop of the capsid protein VP1 is flexible in both variants of the A22 subtype but its overall disposition is distinct from that observed in other FMDV serotypes (O and C). A detailed structural comparison between A22 FMDV and a type O virus suggests that different conformations in a portion of the major antigenic loop of VP1 (the GH loop, which is also central to receptor attachment) result in distinct folds of the adjacent VP3 GH loop. Also, a single mutation (Glu82→Gly) on the surface of VP2 in the suspension-cell-adapted virus appears to perturb the structure of the VP1 GH loop.

Conclusions: The GH loop of VP1 is flexible in three serotypes of FMDV, suggesting that flexibility is important in both antigenic variability and structural communication with other regions of the virus capsid. Our results illustrate two instances of the propagation of structural perturbations across the virion surface: the change in the VP3 GH loop caused by the VP1 GH loop and the Glu82→Gly change in VP2 which we believe perturbs the GH loop of VP1. In the latter case, the amplification of the sequence changes leads to differences, between the monolayer- and suspension-cell-adapted viruses, in host-cell interactions and antigenicity.

Addresses: [1]Pirbright Laboratory, Institute for Animal Health, Ash Road, Pirbright, Surrey, GU24 0NF, UK, [2]Laboratory of Molecular Biophysics, Rex Richards Building, Oxford University, South Parks Road, Oxford OX1 3QU, UK, [3]Wellcome Research Labs, Langley Court, Beckenham, Kent BR3 3BS, UK and [4]Oxford Centre for Molecular Sciences, New Chemistry Laboratory, Oxford OX1 3QT, UK.

[†]Present address: Biophysics Section, Blackett Laboratory, Imperial College, London SW7 2BZ, UK.

*Corresponding author.

Key words: antigenicity, foot-and-mouth disease virus, picornavirus, specificity, X-ray crystallography

Received: **15 Sep 1995**
Revisions requested: **10 Oct 1995**
Revisions received: **16 Nov 1995**
Accepted: **5 Dec 1995**

Structure 15 February 1996, 4:135–145

 ISSN 0969-2126

Introduction

The picornavirus foot-and-mouth disease virus (FMDV) was the first animal virus for which a plurality of serotypes was observed [1]. Seven serotypes (O, A, C, Asia 1 and SAT1–3) and numerous subtypes of FMDV have now been characterized. Antigenic variation occurs across a spectrum, from serotypic variation, where the differences are sufficient to prevent the immune system providing cross protection, to variation in a very small number of amino acids which only affects the binding of a subset of antibodies directed against the virus.

X-ray crystallography has been used to investigate the structural basis of antigenic variation in vertebrate viruses, in particular the membrane proteins of influenza virus [2–5], and of whole picornaviruses [6–13]. Picornaviruses possess an icosahedrally symmetric shell formed by 60 copies of each capsid protein VP1–4. They have a common core structure for their major capsid proteins (VP1–3) consisting of an eight-stranded β-barrel, the strands being labelled alphabetically from B to I (Fig. 1). Structural comparisons between serotypes have been made for poliovirus [8], human rhinovirus [9,11], and FMDV [12]. These studies, which include the analyses of the O and C serotypes of FMDV, have begun to delineate the structural basis of antigenic variation and have shown that for any given picornavirus the surface loops and termini vary between serotypes. However, only one study of more closely related viruses has been reported [13]. Here we compare the structures of two laboratory-grown strains of type A22 Iraq 24/64 FMDV which display significant antigenic variation but differ by only two amino-acid substitutions [14].

Figure 1

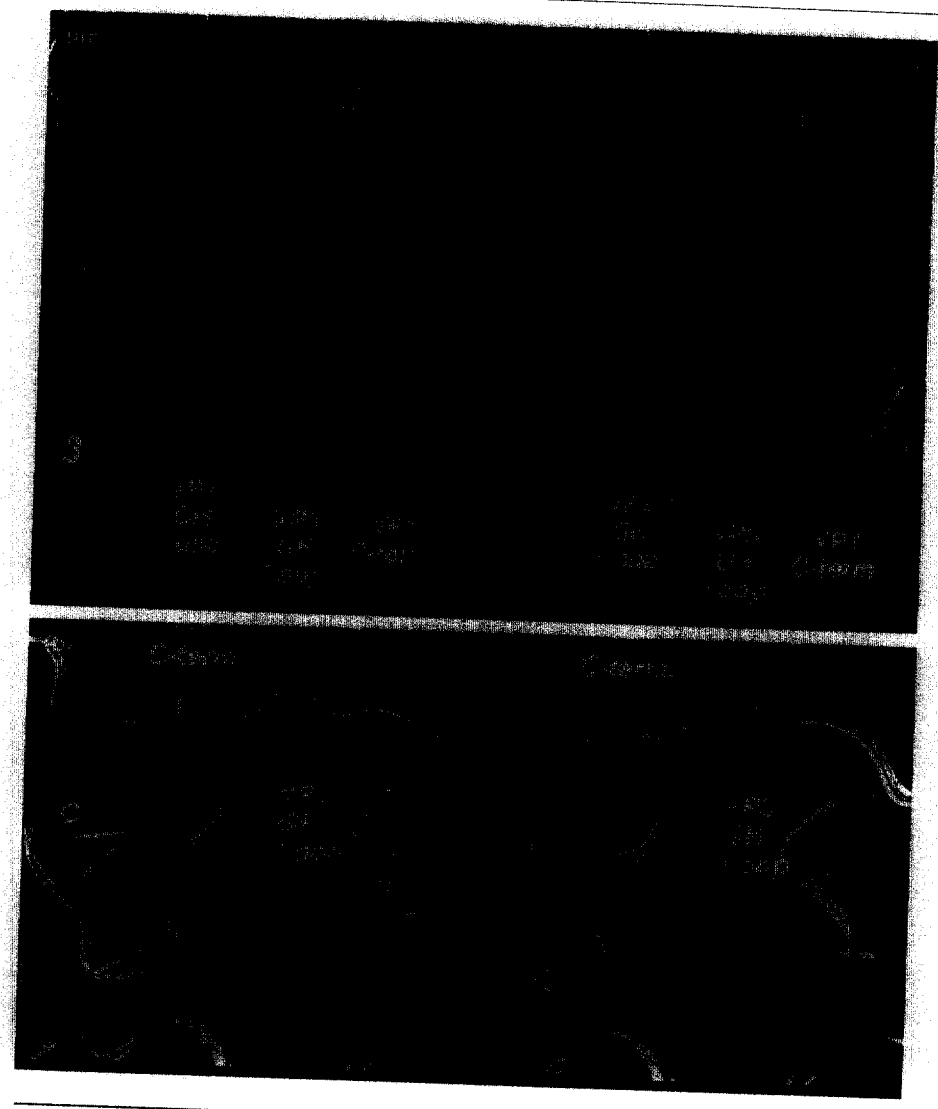

Structure of A22 FMDV and comparison with types O_1BFS and C-S8c1. **(a)** Cα trace of a protomeric subunit of monolayer-cell-adapted A22 FMDV within the context of a pentamer. The protomer is highlighted with thick lines and colour-coded with VP1 in blue, VP2 in green and VP3 in red. The other protomers of the pentamer are depicted with thinner lines and coloured with VP1 in cyan, VP2 in olive green and VP3 in orange. The icosahedral fivefold and threefold symmetry axes are indicated. Note that the N-terminal portion of the VP1 GH loop from one protomer lies adjacent to the VP3 GH loop of a fivefold-related protomer and that the C terminus of VP1 contacts the opposite side of the GH loop of VP3. **(b)** A comparison of the GH loops of VP1 and VP3 for FMDV types A22, O_1BFS and C-S8c1. The image depicts the VP1 GH loop from one protomer and the VP3 GH loop from the fivefold-related protomer within a pentamer. FMDV A22 proteins are shown with thick lines and colour-coded with VP1 in blue, VP2 in green and VP3 in red. The corresponding proteins are shown in orange for O_1BFS and pink for C-S8c1. The N- and C-terminal portions of the GH loop of VP1 are labelled 'N' and 'C' respectively. 'C-term.' indicates the C terminus of VP1 from a fivefold-related protomer.

Although immune selection pressure is commonly cited as a primary cause of antigenic change, other factors, such as viral persistence and adaptation to new cell types, may also be important in influencing antigenicity [15]. These factors have been observed for a number of different viruses: adaptation of influenza to culture *in ovo* [16–18], or of HIV [19] and FMDV [14,20,21] to *in vitro* tissue culture, has been observed to result in antigenic changes. This gives cause for concern about the study of antigenic properties of laboratory-grown viruses. Conversely, antibody mediated selection pressure can affect cell tropism in influenza virus [22,23]. In the case of FMDV, the link between antigenic change and tissue culture adaptation arises because the Arg–Gly–Asp motif in the GH loop of VP1, which is crucial to receptor binding [21,24,25], is flanked by variable sequences which constitute a very important antigenic site on the viral surface [26–29].

The two A22 FMDVs used in this study [14] were selected by passaging in different tissue culture conditions The first, adapted for growth in monolayers of BHK-21 cells, is antigenically similar to the original isolate and isolates from subsequent outbreaks of the disease in the same geographical area [14] . Immunity induced by this strain was broadly effective against a wide range of related strains and so it was considered to be a good candidate vaccine virus [30]. However, adaptation of this monolayer-grown virus to suspension BHK cell culture repeatedly resulted in a variant which displayed significant differences in cell binding, antigenicity and other phenotypic properties [14,31]. Surprisingly, the amino-acid sequence in the VP1 GH loop is identical in the two viruses. The three mutations found in the suspension-cell-adapted virus are all confined to VP2; the two surface-exposed amino-acid changes are hypothesized to alter the virus phenotype by virtue of their effect on the GH loop of VP1 [14].

To investigate the structural consequences of tissue culture adaptation, the structures of the monolayer- and suspension-cell-adapted A22 FMDVs have been determined at 3.0 Å and 2.4 Å resolution, respectively, by X-ray crystallography. The resulting atomic models were refined to the respective R factors of 17.6% and 17.9%. In both viruses, the GH loop of VP1 is flexible but its overall disposition can be distinguished from conformations observed in O and C serotypes of FMDV [10,12]. We present structural evidence which suggests that interaction of the GH loop with other parts of the viral surface can amplify the structural and antigenic effects of sequence variation. Comparison of the monolayer- and suspension-cell-adapted viruses reveals that one of the changes (Glu82 to Gly) on the surface of VP2 perturbs the GH loop of VP1, in what appears to be a further example of amplification, and is the principal determinant of the phenotypic alteration.

Results

Structure of monolayer-cell-adapted A22 FMDV

Comparison with other FMDV structures

The structure of FMDV A22 Iraq (Fig. 1a) is very similar to that reported for type O FMDV [10] and type C FMDV [12]. As expected, the main structural differences between FMDV A22 and the O and C viruses are found in the loops and C termini of VP1–3 that decorate the external surface of the virus. For the cores of the capsid proteins, the root mean square (rms) deviation of Cα positions of the type A virus is only 0.3 Å relative to O_1BFS and 0.4 Å relative to C-S8c1. However, the Cα positions within the surface loops are observed to vary by as much as 12 Å between the three virus serotypes. This is similar to the values found in serotype comparisons of other picornaviruses such as poliovirus [8] and human rhinovirus [9,11], even though the surface loops in FMDV are generally shorter [32].

A comprehensive comparison of the structures of the various aphthoviruses that we have analyzed, and a full discussion of the structural basis of antigenic variation for the aphthoviruses, will be presented elsewhere. Here we will refer to these other viral serotypes only in relation to features which are, so far, peculiar to A22.

The GH loop of VP1

The longest surface loop in A22 FMDV, the GH loop of VP1, does not feature in the electron-density map, presumably because of disordering, therefore residues 137–155, inclusive, are absent from the model. The apparent conservation of flexibility within this region in several FMDV structures [10,12] reinforces the view that conformational variability is an important attribute of the viral surface. However, we can infer that, as well as sequence changes, there are differences in the overall disposition of this loop between the A and O serotypes (Fig. 1b). The residues, at the beginning of the GH loop of VP1 in A22 FMDV (130–136), which are visible in the electron-density map adopt a very different conformation from the visible residues at the beginning of the loop in FMDV O_1BFS (130–134) [10]. This is likely to be caused by the absence, in type A, of a disulphide bridge which, in O_1BFS, pins Cys134 of the VP1 GH loop to Cys130 in VP2. Neither of these cysteines occurs in FMDV A22 and the beginning of the GH loop is free to lie in the opposite direction, pointing away from VP2 and towards VP3 (Fig. 1b). (Reduction of the disulphide bond in dithiothreitol (DTT)-treated O_1BFS allows residues 130–136 of VP1 to adopt a very similar conformation to that observed in A22 [33]; see below.) Similarly, there is no disulphide bond at the start of the GH loop in C-S8c1. However, in this case the density for the loop disappears beyond Gly132 [12] although the apparent difference between this and the GH loop of A22 FMDV may be due to the high temperature factors of the C-S8c1 structure. At the C-terminal end of the loop, where the electron density is again visible for A22, the differences between the three serotypes are less significant (Fig. 1b). Nevertheless, the divergent paths evident at the beginning of the loop strongly suggest that between A and O type viruses there are major conformational alterations in the whole loop that are likely to exceed the maximum observed difference of 12 Å.

Interaction between the GH loops of VP1 and VP3

Adjacent to the VP1 GH loop on the virus surface is the VP3 GH loop from a fivefold-related protomer. Strikingly, in FMDV A22 the fold of the GH loop of VP3 (residues 173–182) is considerably altered from the predominant conformation in O_1BFS [10], although there are no sequence differences between the two viruses in this region (Figs 1b,2). The average shift in Cα position is 4.5 Å. The structural difference between the VP3 GH loops in these two viruses appears to be due to differences in conformation of the adjacent VP1 GH loops.

This interpretation is supported by the observation that treatment of crystals of O_1BFS with 10 mM DTT reduced the disulphide bond between Cys134, at the start of the VP1 GH loop, and Cys130 in VP2, and resulted in the loop adopting a stable conformation that was clearly observed in the electron-density map [33]. In this DTT-treated structure the VP1 GH loop lies predominantly over the surface of VP2; residues 130–136 of VP1 approach the GH loop of VP3 in a fivefold-related protomer and the GH loop of VP3 was observed to be refolded. This refolding was presumably due to the radical shift in the position of the GH loop of VP1, as it does not contain cysteines that might be affected by the presence of DTT (Fig. 2).

In A22 FMDV, residues 130–136, in the GH loop of VP1, and the adjacent GH loop of VP3 adopt conformations that are almost identical to those observed in

Figure 2

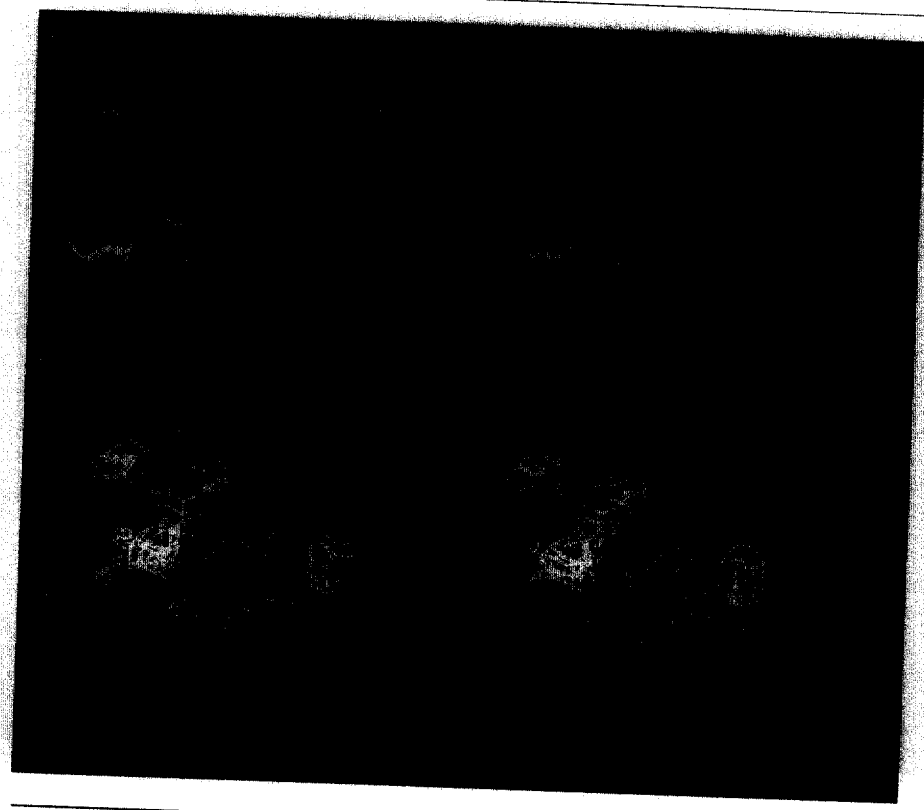

Conformation of the VP1 GH loop affects the VP3 GH loop conformation in a neighbouring protomer. **(a),(b)** A detailed comparison between A22 FMDV and native (a) and DTT-treated (b) O_1BFS FMDV; the diagram compares the interactions of the GH loops of VP1 and VP3 . For A22, residues 130–136 of VP1 are shown in blue, residues 170–175 of VP2 in green and residues 172–181 of VP3 in red. The corresponding portions of native and DTT-treated O_1BFS are shown in cyan, yellow and orange, respectively. For clarity only main-chain atoms are depicted although side chains are included for Tyr136 of VP1, Lys172 of VP2 and Thr178 of VP3 in A22, and for the corresponding residues in O_1BFS (VP1, Tyr136; VP2, Val173; VP3, Thr177). Tyr136 of VP1 is not visible in native O_1BFS as the electron density terminates beyond position 134 in VP1. **(c)** A stereo view of an F_o–F_c omit map for the VP3 GH loop of the parent A22 virus (residues 170–185). The atom trace is shown in red with the electron density contoured at twice the sigma level in green and at the sigma level in light brown. The density suggesting that this loop may also adopt a conformation similar to that observed in untreated O_1BFS, though at very much lower occupancy, is the fragmented brown density looping round to the right of Tyr170 and identified by a white asterisk.

DTT-treated O_1BFS FMDV (Fig. 2b). This finding suggests that the structural factors which determine the shift of the VP3 GH loop upon the reduction of the VP1–VP2 disulphide in O_1BFS also determine the structural difference in this region between native O_1BFS and A22. A factor allowing the shift is the absence of a disulphide bond fixing the start of the VP1 GH loop to VP2 and the burial of Tyr136 of VP1 is likely to be a significant driving force. In A22, the side chain of this tyrosine is contained within an amphiphilic pocket formed by amino acids from VP2 and VP3. Residues 176–178 of VP3, which line one side of the pocket, are contained within the GH loop of VP3. In DTT-treated O_1BFS, Tyr136 of VP1 is slightly more buried, possibly due to the presence of a valine rather than a lysine at position 173 in VP2, which, between the two viruses, is the only sequence difference in the pocket. In A22 the side chain of Lys173 sterically prevents Tyr136 descending further into the pocket (Fig. 2b). Further differences between the VP1 GH loops and other surface features of the two viruses may also be involved; for example, residues 190–200 in the C-terminal portion of VP1, which vary between serotypes, also pack against the GH loop of VP3 (Fig. 1). In A22 FMDV the VP3 GH loop is quite mobile, as indicated by the high B factors for this portion of the model (the average B factor for the main-chain atoms of residues 173–182 is 54.9 Å^2). In fact an F_o–F_c omit map for A22 suggests that the GH loop of VP3 may also adopt a conformation similar to that observed in untreated O_1BFS, although at very much lower occupancy (Fig. 2c). The conformational switching of this region in A22 may well be linked to movements of the flexible VP1 GH loop (the average B factor for the main-chain atoms of residues 130–136 is 47.1 Å^2).

Given this evidence that the GH loops of VP1 and VP3 interact, the observation that the dominant conformation of the GH loop of VP3 in C-S8c1 FMDV is similar to that in the native O_1BFS but different to that in type A22 (Fig. 2b) suggests that there are differences between A22 and C-S8c1 in the disposition of the VP1 GH loops.

Structure of the suspension-cell-adapted A22 variant

The structure described above is for a virus which was plaque purified from a stock that had been passaged 13 times in BHK-21 cell monolayers. The suspension-cell-adapted variant of FMDV A22 was generated by three passages of the monolayer-cell-adapted virus stock in BHK-21 suspension cells; it was also plaque purified [14]. The variant displays cell-binding and antigenic properties distinct from those of the parental monolayer-cell-adapted A22 virus [14]. It was originally anticipated that the variant would contain mutations in the GH loop of VP1, which contains the primary determinant for interaction with the cellular receptor [21,24,25] and is a prominent antigenic feature on the viral surface [10,34–36]. However, the sequence reported for the variant [14] contained only

Figure 3

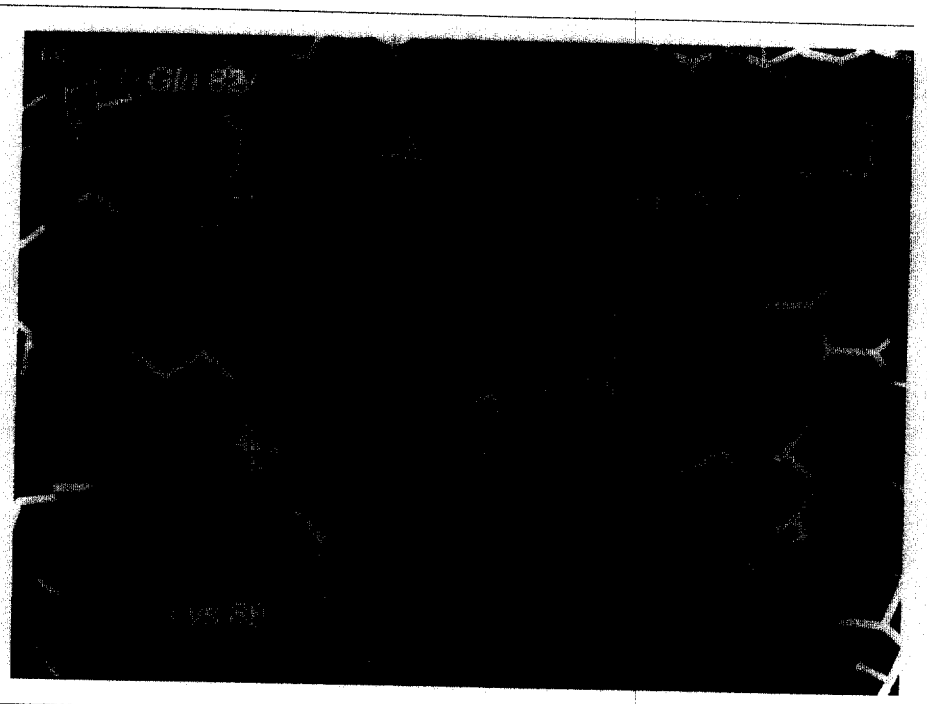

F_o^{var}–F_o^{par} difference density superimposed on the model of monolayer-adapted A22 FMDV illustrating side-chain differences between monolayer- and suspension-cell-adapted A22 FMDV. **(a)** The negative density contours shown in orange indicate replacement, at position 82 in VP2, of glutamate by glycine in the suspension-cell-adapted variant . However, there is no difference density to suggest the replacement in the variant of lysine by threonine at position 88 in VP2. **(b)** Positive density contours in green confirm the replacement of histidine at position 207 in VP2 by tyrosine in the variant. Beneath this residue, positive density indicates increased ordering of Glu40, Asp41 and, to a lesser extent, His42 of VP2 in the suspension-cell-adapted virus.

three mutations, all of them located in VP2 although lying in close proximity to the VP1 GH loop. It has been speculated that one or two of these mutations might affect the VP1 GH loop structure and thus account for the altered phenotype [31].

The difference electron density map F_o^{var}–F_o^{par}, calculated using phases from averaging the parental map, bears clear evidence for two of the three reported mutations in VP2. There is a negative density feature at the location of the side chain of Glu82 consistent with the substitution of a glycine in the variant (Fig. 3a). A peak of positive density confirmed the replacement of His207 by a tyrosine residue (Fig. 3b). However, there was no density to support the mutation of Lys88 to threonine (Fig. 3a) and a $2F_o^{var}$–F_o^{par} map clearly indicated that lysine remained at position 88. This was confirmed by sequencing cDNA derived from the viral RNA. Despite this apparent reversion, the variant strain used in this study retained the distinctive ability to infect suspension cells as described by Bolwell and colleagues (data not shown) [14].

The $2F_o^{var}$–F_c^{var} map (calculated with model phases after refinement and 15-fold averaged) contains other interesting features. Most notable is the presence of additional density indicative of increased order in portions of the VP1 GH loop. In the parent virus structure, density corresponding to residues 137 to 155, inclusive, was absent from the map. In the variant map, the electron density permitted inclusion of Ser137 at the start of the GH loop. An F_o^{var}–F_c^{var} omit map calculated with a phasing model lacking residues 130–137 of VP1 and residues 170–185 of the adjacent VP3 GH loop confirmed the presence of Ser137 (Fig. 4). There is also additional density attached to the carbonyl oxygen of Leu66 in VP2. Close to this leucine the side-chain density of Glu79 in VP2 is significantly stronger indicating greater ordering of this residue in the variant than in the parental structure. The side-chain of Lys88 in VP2 also appears more ordered, as does the Glu218 at the C terminus of the twofold-related VP2, which lies only 3.5 Å from Lys88. Although these indications do not permit construction of a model, they suggest that portions of the VP1 GH loop may be more ordered in the variant and more closely associated with the surface of VP2, in a conformation somewhat akin to the loop structure in DTT-treated O_1BFS [33]. Conversely, there is no density to support inclusion of Ala156 at the C-terminal portion of the VP1 GH loop, suggesting that this minor part of the GH loop may be more disordered in the variant than in the parent.

The two sets of diffraction data are of differing quality, completeness and resolution, with the variant data being sparse at higher resolution (Table 1). However, the fact that some residues are observed to be more ordered in one structure and some more ordered in the other suggests that these features are genuinely significant. Moreover, when the $2F_o$–F_c maps for parent and variant are adjusted to give coincident contours for the side chains of buried residues the additional features exposed on the surface of VP2 are still evident, again suggesting that they are real. Finally, we have independently determined the structure of the A22 empty capsid and observe no such differences in the VP1 GH loop structure (unpublished results).

Figure 4

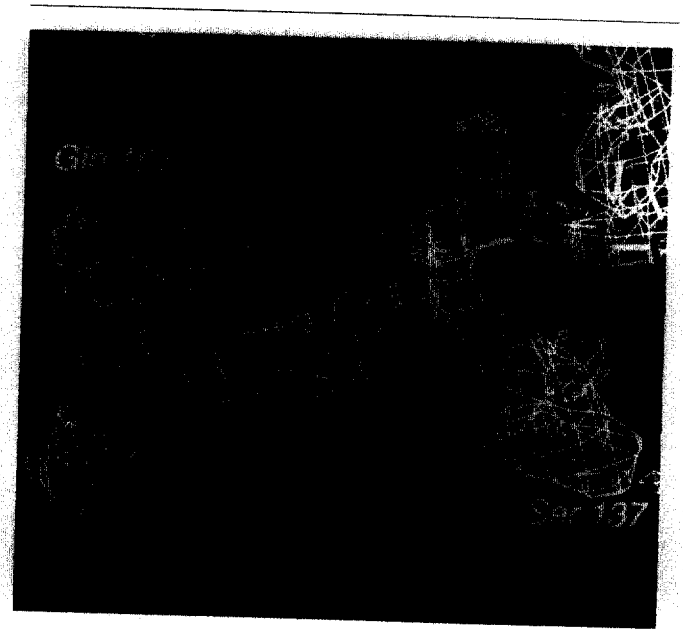

An F_o–F_c omit map calculated for the suspension-cell-adapted variant of A22 FMDV. Residues 130–137 in the GH loop of VP1 and 170–183 in the GH loop of VP3 were omitted from the model used to calculate the phases. The resulting density confirms the model for residue 137 in VP1. Gln157 is the first residue visible in a $2F_o$–F_c map at the C-terminal portion of the VP1 GH loop.

Table 1

Data processing and model refinement statistics.

	Monolayer-cell-adapted virus	Suspension-cell-adapted virus
Data processing		
Number of films	22	0
Number of images	64	16
Total reflections	483 707	120 353
Independent reflections	251 190	110 781
Completeness (outer shell) [%]	61.7 (21.1)	14.1 (3.5)
R_{merge}* (outer shell) [%]	17.9 (35.2)	9.6 (27.5)
C_{AV}†	0.976	–
R_{AV}‡	21.9%	–
Refinement		
Range of spacings (Å)	25–3	17–2.4
Total non-hydrogen atoms	5200	5202
Solvent sites	310	243
R_{model}§ (all data)	17.6	17.9
Δ_{bonds}# (Å)	0.015	0.015
Δ_{angles}** (°)	1.91	1.94
ΔB bonds†† (Å²)	2.15	2.29
ΔB angles‡‡ (Å²)	3.64	3.66
Average B (Å²)	17.0	17.6

*$R_{merge}=[\sum_h \sum_i |(I_h - I_{hi})|]/[\sum_h \sum_i I_{hi}] \times 100$

†$C_{AV}=\frac{\sum_h (\bar{F}_{obs}-|F_{h,obs}|)(\bar{F}_{av}-|F_{h,av}|)}{[\sum_h (\bar{F}_{obs}-|F_{h,obs}|)^2 . \sum_h (\bar{F}_{av}-|F_{h,av}|)^2]^{1/2}}$

‡$R_{AV}=\frac{\sum_h |(|F_{h,obs}|-|F_{h,av}|)|}{\sum_h |F_{h,obs}|} \times 100$

§$R_{model}=\frac{\sum_h |(|F_{h,obs}|-|F_{h,calc}|)|}{\sum_h |F_{h,obs}|} \times 100$

#Rmsd from ideal covalent bond lengths. **Rmsd from ideal covalent bond angles. ††Rmsd of B factors for the bond restraints. ‡‡Rmsd of B factors for the angle restraints. For the monolayer-cell-adapted virus, some 88% of the residues lie in the most favoured region of the Ramachandran plot and none in disallowed regions. For the suspension-cell-adapted virus, some 89% of the residues lie in the most favoured region of the Ramachandran plot and none are in disallowed regions.

The structural differences in the VP1 GH loop, between the parent and variant, are relatively minor and the apparently greater stability of the loop in the variant is slight. For both viruses the VP1 GH loops are very flexible. Antigenic differences between the two viruses in this region may simply result from the expression of different sets of loop conformations.

Curiously, the BC loop of VP3 in the variant shows a clear difference from the parent. This loop, which is the most surface exposed loop on VP3 (located at the bottom right of the protomer shown in Fig. 5), appears to adopt two conformations in the variant, one of which is similar to the conformation found in the parent (and in C-S8c1); the other (which is better occupied and therefore included in the model) is similar to the conformation found in O_1BFS [10]. This difference is hard to explain as there are no reported sequence differences between the parent and variant in the BC loop or adjacent portions of the structure. The variant was crystallized at a slightly lower ionic strength and in the presence of 1,4-dioxane, either of which may account for variation in the VP3 BC loop, but the packing interactions in the crystals of the wild-type and variant viruses were identical and structures of FMDV O_1BFS in ammonium sulphate and PEG were indistinguishable from each other (unpublished results). Alternatively the differences in the conformations of the VP1 GH loop in the monolayer- and suspension-cell-adapted viruses may affect the VP3 BC loop structure; the length of the flexible portion of the VP1 GH loop is indeed sufficient to allow it to contact a threefold-related BC loop of VP3.

One other unexpected difference between variant and parent is the relative ordering of residues 40–42 in VP2 of the variant. This segment is located at the interior face of the capsid, immediately adjacent to the viral RNA. The side chain of Glu40 lies only 3.9 Å from residue 207 in VP2 which is mutated from a histidine to a tyrosine in the suspension-cell-adapted variant (Fig. 3b). It may be that the interaction with the surrounding RNA is affected in the variant, constraining residues 40–42.

Discussion

Novel features of A22 FMDV

The exposed, flexible GH loop of VP1 of FMDV contains a strictly conserved motif (Arg–Gly–Asp) which is primarily

responsible for binding the virus to its cellular receptor [21,24,25] . No density was observed for most of the VP1 GH loop of type A22 FMDV consistent with the structures of type O and C FMDV [10,12]. Nevertheless, differences in the structures and orientations of the visible portions at the beginning and end of the loop indicate that serotype-specific dispositions are adopted in type O, C and A viruses (Fig. 1b). Distinct sets of loop conformations may characterize each serotype. Recent studies shed some light on the nature of these differences. The structure of an antibody Fab fragment bound to a peptide corresponding to the VP1 GH loop of a type C FMDV showed the internal structure of the loop to be strikingly similar to that in the DTT-treated type O_1BFS virus (in which the whole loop is clearly visible), despite significant sequence variation between the two serotypes [37]. Another investigation with DTT-treated variants of type O_1 FMDV found that mutations within the loop had no observable effect on the main-chain structure and suggested that the loop may be able to move in the native virus as a hinged unit that has significant internal stability [13]. The diverse conformations of this loop noted above for O, A and C serotypes may therefore be due, in part, to differences in the preferred orientation of this unit.

In contrast, although the amino-acid sequences of the VP3 GH loop of A22 and O_1BFS FMDV are identical, this loop adopts distinct folds in the two viruses (Fig. 2), apparently due to different conformations of the VP1 GH loops in these two serotypes. This loop is an antigenic feature of the virus [29], therefore the observed conformational changes appear to amplify the antigenic impact of sequence and structural variation within the GH loop of VP1. Further instances have been reported in which interactions of the GH loop of VP1 with other parts of the viral surface leads to potential amplification of antigenic variation (Fig. 5). Variants of O_1BFS FMDV, raised under the selective pressure of a monoclonal antibody which recognised part of the VP1 GH loop, contained mutations, not in the GH loop, but in the BC loop of VP1 [38], which is itself an antigenic site [28]. Differences in the structure of the VP1 GH loop of these variants were indeed observed, presumably due to the side-chain substitutions in the BC loop [38]. In another study, a mutation in VP2 (position 80) of FMDV A10 Holland was found to abrogate recognition by some monoclonal antibodies directed against the GH loop of VP1 [27]. Finally, in the viruses which are the subject of this paper, a mutation in VP2, generated by adaptation of the virus to suspension-cell culture, leads to altered antigenicity of the GH loop of VP1 [31,39]. Clearly, point mutations on the virus surface can have a very significant impact on the VP1 GH loop structure. We now find that a reciprocal effect also occurs, the VP1 GH loop affecting the conformation and antigenicity of an adjoining feature, the GH loop of VP3. The flexibility of the GH loop of VP1 may have two roles in promoting antigenic variation: as well as permitting a high degree of sequence variability, it seems to facilitate structural 'cross-talk' with other regions of the capsid surface.

Figure 5

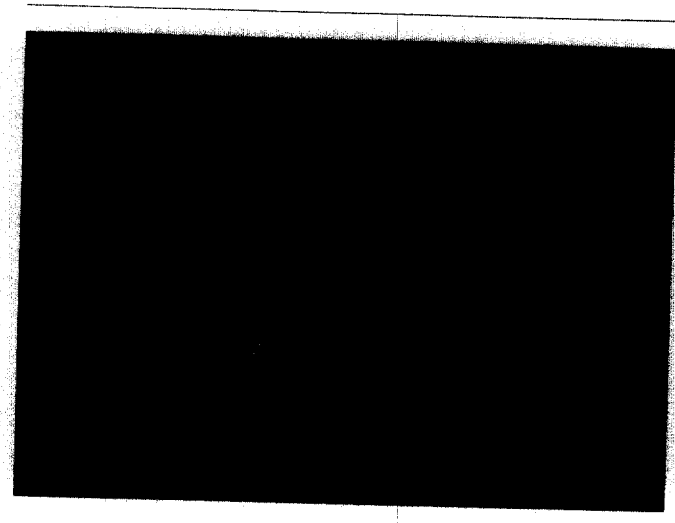

Residues which are reported to influence, or be influenced by, the GH loop of VP1. A Cα trace for a single copy of VP1 (blue), VP2 (green) and VP3 (red) of monolayer-cell-adapted A22 FMDV is shown. The C terminus of VP1 from a fivefold-related protomer is depicted in cyan. The conformation of the GH loop in DTT-treated O_1BFS FMDV is depicted in yellow. Space filling models of side-chain atoms indicate the positions of residues which affect the structure of the GH loop of VP1: in VP1, 43, 48, 59 (see [41]); in VP2, 80 (see [27]) and 82 and 88 [14]; in VP3 residues 175–183 (this work). The residue labels are colour-coded as for the proteins.

In spite of these advantages, long flexible loops are observed infrequently in nature. A potential disadvantage of the greater flexibility displayed by FMDV is susceptibility to proteolysis. Thus, in poliovirus, for example, all of the surface loops were resolved in the crystal structures [7,8] although even here there is evidence for structural cross-talk involving an antigenic site [8]. This increased rigidity may be linked to the fact that poliovirus, unlike FMDV, must endure passage through the gut in order to replicate; however, there may also be a further reason. Interaction of poliovirus with its cellular receptor leads to a concerted conformational change in the virus capsid as a pre-requisite to uncoating. The mechanics of biological function thereby require some rigidity to drive the transition, whereas in FMDV acidification is sufficient to initiate uncoating.

Structure of a suspension-cell-adapted variant

Although some viruses, such as human rhinovirus (HRV), appear to have successfully separated determinants of cell tropism from important antigenic sites [6], features which are necessarily located on the external surfaces of viral proteins, others sustain a closer physical association of these functions. Interdependence of the two functions inevitably results. The V3 domain of the gp120 glycoprotein in HIV,

for example, is a key determinant of cell tropism [40–42] and is the site of a proteolytic cleavage thought to be required for infection [43–45]. The same domain has been identified as an important antigenic and immunogenic feature of HIV [46,47]. Similarly, in FMDV the conserved Arg–Gly–Asp receptor-binding motif of the GH loop of VP1 [21,24,25] is flanked on both sides by hypervariable sequences that constitute the most intensively studied antigenic sites on the viral capsid [34–36,48]. Consequently, adaptation of FMDV to different growth conditions often leads to sequence and antigenic variation [20,49]. Sequence changes have most often been observed in the GH loop of VP1 itself. However, adaptation of the monolayer-cell-adapted stock of FMDV A22 to suspension-cell culture resulted in a variant containing three amino-acid changes in VP2 [14]. The variant bound to both monolayer and suspension cells better than the monolayer-adapted parental strain but had a small plaque phenotype and displayed a tendency to aggregate [14]. Moreover, although antisera raised with the monolayer-adapted virus neutralized a wide range of field strains of serotype A FMDV, antisera raised using the variant was much less effective against heterologous viruses although it was a potent immunogen for homotypic responses (the suspension virus always induced higher levels of antibody) [14,30,31]. Curiously, however, monoclonal antibodies produced against the monolayer-cell-adapted virus, most of which recognised the GH loop of VP1, generally had higher neutralization titres against the variant [14]. On the basis of the structure of a type O virus, which shares 70% amino-acid-sequence homology with type A FMDV, it was suggested that the two mutations located on the exterior of VP2 (Glu82→Gly and Lys88→Thr) would be principal determinants of the altered antigenic and cell-binding properties of the variant [31] and would act by influencing the structure of the GH loop of VP1.

The structure of suspension-cell-adapted FMDV A22 presented here contains only two of the three mutations reported [14] and only one of the two found on the exterior surface of VP2 (Fig. 3). Nevertheless, it appears to share the same phenotype as the virus isolated by Bolwell and colleagues [14]. The surface mutation (Glu82→Gly) is located close to the GH loop of VP1 and therefore appears to be key to the phenotype of the suspension-cell-adapted variant (Fig. 5). In DTT-treated serotype O virus, where the loop adopts a stable conformation [33], Glu82 (which is conserved between O and A type FMDV) makes three hydrogen bonds with the GH loop. Although in the parental monolayer-cell-adapted A22 FMDV the GH loop is largely disordered, it shares some similarity with the DTT-treated O_1BFS loop structure and appears to lie predominantly over VP2. The loss of the glutamate side chain in the suspension-cell-adapted variant of A22 has relatively little observable impact on the structure of the GH loop of VP1. The visible N-terminal end (residues 130–137) appears somewhat more stable (Fig. 4) and there is evidence of greater interaction with the surface of VP2. This is surprising given the evident stabilizing effect of Glu82 in DTT-treated O_1BFS. The C-terminal portion of the loop is less stable. It seems likely that mutations on the surface of VP2 alter the balance of forces on the GH loop so that a different ensemble of conformations is favoured.

Although the nature of the differences in the receptors for FMDV between monolayer and suspension BHK-21 cells is unknown, it is likely that the suspension cells display a different array of integrins. The suspension-cell-adapted variant binds better to both cell types, suggesting that either this virus can recognize a different, higher titre, receptor present on both cell lines, or, alternatively, the parent virus is unable to bind to the receptor used on suspension cells, restricting it to an integrin on the monolayer cells.

The subtle structural changes between monolayer- and suspension-cell-adapted A22 FMDVs confer distinct antigenic properties. Access to residue 82 of VP2 is likely to be obscured by the overlying GH loop of VP1; the main antigenic differences therefore appear to be attributable to the changes induced in the VP1 GH loop of the variant. (Glu82 is relatively buried in the structure having a fractional accessibility of 0.23 calculated using QUANTA [Molecular Simulations] compared with 0.86 for Glu131 of VP2 and 0.83 for Glu59 of VP3, which are both located at antigenic sites.) This is supported by the observation that monoclonal antibodies (mAbs) raised against the parent bind the variant at least as tightly, arguing against a specific interaction between the glutamate and the mAbs [14]. Antibodies are exquisitely sensitive to structural variation, a simple side-chain difference often being sufficient to greatly impair binding [4,28]. In the worst case a single substitution can result in an ineffective vaccine [18]. This, together with the disorder in the GH loop of VP1, makes it difficult to conclusively demonstrate the mechanism underlying the puzzling antigenic properties of these viruses [14,31], although the greater apparent stability of the VP1 GH loop in the suspension-cell-adapted variant suggests a possible explanation. Thus, monoclonal antibodies raised against the monolayer-cell-adapted virus (parent) and which bind to the GH loop of VP1 are generally more effective against the variant than against the parent [14]. This is consistent with greater stability of part of the VP1 GH loop in the variant which reduces the entropic cost of antibody binding. Conversely, antiserum raised by the variant neutralizes the variant with a titre 12- to 50-fold higher than it does the parent [14,39]. Again, entropy may provide at least a partial explanation, the greater flexibility of the GH loop in the parent viruses increasing the entropic cost of binding.

Biological implications

Antigenic variation between the seven serotypes of the picornavirus foot-and-mouth disease virus (FMDV) poses difficulties in controlling the disease by vaccination. Moreover, tissue-culture adaptation of viruses, which is frequently required for large-scale vaccine production, can give rise to further antigenic variation which may compromise vaccine effectiveness. Picornaviruses comprise four capsid proteins, VP1–4. The interdependence of anti genicity and host-cell specificity arises in FMDV because a single extended loop on the viral surface — the GH loop of VP1 — not only contains the Arg–Gly–Asp motif required for receptor binding but also comprises an important antigenic site. In the case of a type A22 FMDV, merely adapting the virus from monolayer- to suspension-BHK cell culture resulted in a variant that displayed differences in cell-binding properties and antigenicity as a consequence of three amino-acid substitutions in the capsid protein VP2. However, these differences arose because of mutations outside the VP1 GH loop suggesting that interactions between the loop and other parts of the viral capsid could affect its structure and function.

Comparison of monolayer- and suspension-cell-adapted A22 FMDVs shows that a single mutation (Glu82→Gly) on the surface of VP2 in the suspension-cell-adapted virus appears to perturb the structure of the VP1 GH loop causing stabilization at the N-terminal and destabilization at the C-terminal portions of the loop. This appears to be the principal determinant of the differences in the variant's host-cell interactions and antigenicity.

These viruses belong to the third FMDV serotype (A) to be structurally characterized and our results reveal significant differences in the surface structure of each serotype. In common with type O and C FMDVs, the GH loop of VP1 of a type A virus is very flexible and the largest differences between serotypes are associated with this loop. The flexibility of the VP1 GH loop allows considerable sequence and antigenic variation around the conserved receptor-binding motif. We have found that this loop flexibility may also be exploited to amplify the structural effects of sequence changes. In addition to the case mentioned above, comparison of the structures of A22 with type O FMDV indicated that the conformation of the GH loop of VP1 profoundly affects the structure adopted by the GH loop of VP3 in an adjoining protomer; this extends the impact of sequence and structural variation in the VP1 GH loop even though the VP3 GH loop sequences in the two viruses are identical.

Materials and methods

Virus growth, purification and crystallization

The monolayer-cell-adapted clone of FMDV A22 Iraq 24/64 (162–154) and the suspension-cell-adapted clone (148–173) [14] were kindly supplied by Dr EJ Ouldridge. The suspension-cell-adapted (variant) virus was grown in roller bottles of BHK-21 monolayers as it is known to propagate in monolayers as efficiently as the parental virus [14]. The propagation, purification and crystallization of the monolayer-cell-adapted (parental) virus has been described [50]. Because of the tendency of the variant to aggregate during purification, a modification of the purification procedure was developed. Briefly, upon attaining full cytopathic effect the infected cells were lysed with 40 mM Tris, 300 mM NaCl, pH 7.6 (buffer A) containing 0.1% (v/v) Triton X-100. Virus precipitated with $(NH_4)_2SO_4$ was resuspended in buffer A containing 0.1% (v/v) Triton X-100. Material that was not resuspended was removed by centrifugation and the virus pelleted through a cushion of 30% (w/v) sucrose in buffer A at 141 000 × g, 4°C for 150 min. The virus pellets were soaked overnight in buffer A and then treated with 0.1 mg ml^{-1} RNase and 0.2% (v/v) Triton X-100 before ultracentrifugation through 15–45% (w/v) sucrose gradients containing 2.5 M NH_4Cl, 40 mM Tris, pH 7.6 at 141 000 × g, 12°C, for 3.5 h. Fractions containing virus were pooled and diluted with an equal volume of 2.5 M NH_4Cl, 40 mM Tris, pH 7.6 and the virus pelleted finally at 275 000 × g for 3 h at 12°C, through 30% (w/v) sucrose containing the same buffer. The virus was resuspended at a concentration of 10 mg ml^{-1} in 1.0 M NH_4Cl, 40 mM Tris, 3 mM NaN_3, pH 7.6 and stored at 4°C.

Crystals of the suspension-cell-adapted variant were obtained by sitting drop vapour diffusion in microbridges [51]. Typically 5 µl of 10 mg ml^{-1} virus was mixed with 5 µl from the reservoir. The virus crystallized in 3.8–4.5% (w/v) polyethylene glycol (PEG) 20000 containing 2.5 M NH_4Cl, 4% (v/v) 1,4-dioxane, 0.1 M sodium phosphate, pH 7.6 at 21°C. Very similar conditions, but with 4 M rather than 2.5 M NH_4Cl and lacking 1,4-dioxane, were used to crystallize the parent virus and empty capsids [50]. Crystal yields and sizes were improved by micro- and macroseeding [52]. Three crystal habits were observed under our crystallization conditions: Type I, truncated triangular prisms; Type II, hexagonal prisms with scooped patterns on the hexagonal faces; Type III, irregular pentagonal prisms, which appeared to be truncated versions of type II that lacked their surface 'scoops'. All of the variant habits differed from those observed with parental virus. Types I and II gave disordered diffraction; Type III crystals diffracted to 2.4 Å resolution and were used for data collection. They were found to have the same space group (I222) and cell dimensions as the parental virus crystals (see below).

Data collection and processing

X-ray data collection for parental virus, performed at the SERC Synchrotron Radiation Source, Daresbury, UK, has been described [50]. For crystals of the A22 suspension-cell-adapted variant the data were also collected at Daresbury using similar protocols. In this case however, the data were recorded on the Rigaku R-Axis II imaging plate device installed on station 9.6. Diffraction data for the parental virus were collected on CEA X-ray film and on a Marresearch Hendrix-Lentfer imaging plate device on stations 9.6 and 9.5. Both imaging devices enabled multiple exposures (5–35) from each crystal in contrast to film with which a maximum of 2 exposures per crystal were obtained. Film data were processed as described previously [53]. Image plate data were processed using MOSFILM (A Leslie, unpublished program). The data were merged and scaled using ROTAVATA and AGROVATA and post refined with POSTREF, all programs from the CCP4 package [54]. Reflections which were more than 70% recorded were scaled appropriately and treated as fully recorded. R_{merge} values for the parent and variant data were 17.7% and 9.6%, respectively (Table 1). The low R_{merge} of the variant data reflects the fact that they were collected from a single well-diffracting crystal and also the much lower redundancy in the data.

Figure 6

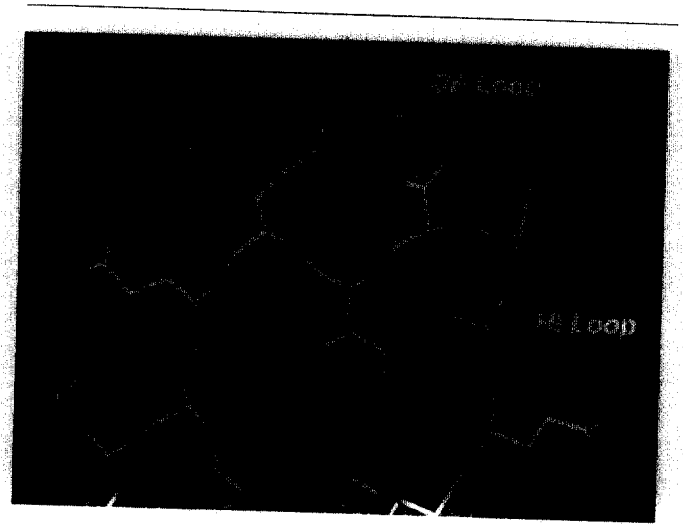

Typical electron density from the $2F_o-F_c$ map for monolayer-cell-adapted A22 FMDV calculated with phases refined by cyclic 15-fold non-crystallographic averaging. The portion shown includes the DE and HI loops which are exposed on the surface of VP1 close to the fivefold symmetry axis at the centre of a pentamer.

Structure determination of the monolayer-cell-adapted virus

A self-rotation function was calculated for the parental A22 FMDV data using POLARRFN from the CCP4 package in order to resolve the ambiguity in the orientation of the icosahedral virion in the I222 unit cell. With this information, a model of O_1BFS FMDV was placed at position 0,0,0 and used in a rigid body grid search with X-PLOR [55] to refine the cell dimensions. These were found to be a=328.2 Å, b=341.2 Å and c=363.7 Å.

Initial phases were calculated by placing an unrefined model of $A10_{61}$ FMDV (Fry *et al.*, unpublished data) in the unit cell. $2F_{obs}-F_{calc}$ and $F_{obs}-F_{calc}$ maps were calculated using these phases and put through one cycle of 15-fold noncrystallographic averaging using an early version of GAP (J Grimes and DS, unpublished program]. The resulting map was of high quality: the amino acid differences between $A10_{61}$ and A22 Iraq FMDV were very evident indicating a lack of bias towards the $A10_{61}$ model. An initial model for the parental A22 virus was built into this map using FRODO [56] and refined with X-PLOR. The model used in the refinement contained a bulk solvent correction calculated with solrad= 0.1 Å, k_{solv}=0.35 and B_{solv}=50 Å^2, values which were determined to be optimal for the A22 data set. Throughout refinement strict noncrystallographic symmetry constraints and the parameter set of Engh and Huber [57] were used. Phases calculated from the refined model were refined by a further cycle of noncrystallographic symmetry averaging. A second round of model building and refinement followed. At this point a $2F_{obs}-F_{calc}$ map calculated using model phases was averaged to convergence with GAP. The final correlation coefficient, C_{AV}, for this map was 0.967 and R_{AV} was 21.9% (Table 1; Fig. 6). Using the phases refined by averaging, $2F_{obs}-F_{calc}$ and $F_{obs}-F_{calc}$ maps were calculated in order to make minor adjustments to the model before final positional and B-factor refinement with X-PLOR. Subsequently, 310 water molecules have been added and the final refinement statistics are given in Table 1. The model lacks residues 137–155 and 211 of VP1, 1–11 of VP2 and 1–14 and 40–64 of VP4.

Structure determination of the suspension-cell-adapted virus

For the variant, $2F_o^{var}-F_o^{par}$ and $F_o^{var}-F_o^{par}$ maps were calculated using the parental phases from the cyclic averaging; F_o^{par} and F_o^{var} are the observed structure factors for the parent and variant respectively. These maps were then subjected to a single cycle of noncrystallographic symmetry averaging. The model of the monolayer-cell-adapted A22 FMDV was used as a starting point for model building. The model was subjected to positional and B-factor refinement with X-PLOR. $2F_o-F_c$ and F_o-F_c maps calculated with model phases were used to make adjustments to the model and to add 243 water molecules before final positional and B-factor refinement (Table 1). The variant model lacks residues 138–156 and 211 of VP1, 1–11 of VP2 and 1–14 and 40–64 of VP4.

Molecular graphics

Model building was performed using FRODO [56]. Figures were prepared with O [58] and Photoshop (Adobe).

cDNA sequencing

Single-stranded cDNA was synthesized from purified viral RNA using reverse transcriptase and oligo A22F (5′-CTGGTTGCCAACAGCGGA-3′; VP2 nucleotides 600–583). The VP2 coding sequence containing codons for two of the mutations in the variant was amplified using oligos A22F and A22R (5′-CAGGCAGAAAGATTT-TTC-3′; VP2 nucleotides 441–424) in the polymerase chain reaction and cloned in to the vector pGEMt (Promega). Three independent amplifications were sequenced in both directions.

Coordinates have been deposited with the Brookhaven Protein Data Bank.

Acknowledgements

We thank David Goodrich for his time on data collection trips as disease security officer and the staff of the Synchrotron Radiation Source, Daresbury Laboratory for practical assistance, Stephen Lee for photography and Richard Bryan computing. We are grateful to Dr E Ouldridge (Pittman-Moore) for the gift of infecting stocks of both viruses used in this study. EF was supported by the MRC. RA, WB, SC, TJ and SL were supported by the BBSRC and SL also by the OCMS.

References

1. Vallée, H. & Carre, H. (1922). Sur la pluralité du virus aphteux. *C. r. hebed. Seanc. Acad. Sci., Paris.* **174**, 1498–1500.
2. Colman, P.M. (1992). Structural basis of antigenic variation: Studies of influenza virus neuraminidase. *Immunol. Cell. Biol.* **70**, 209–214.
3. Knossow, M., Daniels, R.S., Douglas, A.R., Skehel, J.J. & Wiley, D.C. (1984). Three-dimensional structure of an antigenic mutant of the influenza virus hemagglutinin. *Nature* **311**, 678–700.
4. Tulip, W.R., *et al.*, & Colman, P.M. (1991). Refined atomic structures of N9 subtype influenza virus neuraminidase and escape mutants. *J. Mol. Biol.* **221**, 487–497.
5. Wiley, D.C. & Skehel, J.J. (1987). The structure and function of the hemagglutinin membrane glycoprotein of influenza virus. *Annu. Rev. Biochem.* **56**, 365–394.
6. Rossmann, M.G., *et al.*, & Vriend, G. (1985). Structure of a human common cold virus and functional relationship to other picornaviruses. *Nature* **317**, 145–153.
7. Hogle, J.M., Chow, M. & Filman, D.J. (1985). Three-dimensional structure of poliovirus at 2.9 Å resolution. *Science* **229**, 1358–1365.
8. Filman, D.J., Syed, R., Chow, M., Macadam, A.J., Minor, P.D. & Hogle, J.M. (1989). Structural factors that control conformational transitions and serotype specificity in type 3 poliovirus. *EMBO J.* **8**, 1567–1579.
9. Kim, S., *et al.*, & McKinlay, M. (1989). Crystal structure of human rhinovirus serotype 1A (HRV1A). *J. Mol. Biol.* **210**, 91–111.
10. Acharya, R., Fry, E., Stuart, D., Fox, G., Rowlands, D. & Brown, F. (1989). The three-dimensional structure of foot-and-mouth disease virus at 2.9 Å resolution. *Nature* **337**, 709–716.
11. Oliveira, M.A., *et al.*, & Rossmann, M.G. (1993). The structure of human rhinovirus 16. *Structure* **1**, 51–68.
12. Lea, S., *et al.*, & Mateu, M. G. (1994). The structure and antigenicity of a type C foot-and-mouth disease virus. *Structure* **2**, 123–139.
13. Lea, S., *et al.*, & Stuart, D. (1995). Structural comparison of two strains of foot-and-mouth disease virus subtype O_1 and a laboratory antigenic variant, G67. *Structure* **3**, 571–580.
14. Bolwell, C., *et al.*, & Rowlands, D.J. (1989). Host cell selection of antigenic variants of foot-and-mouth disease virus. *J. Gen. Virol.* **70**, 45–57.

15. Domingo, E., *et al.*, & Mateu, M. (1993). New observations on antigenic diversification of RNA viruses. Antigenic variation is not dependent on immune selection. *J. Gen. Virol.* **74**, 2039–2045.
16. Robertson, J.S., *et al.*, & Schild, G.C. (1987). Structural changes in the haemagglutinin which accompany egg adaptation of an influenza A(H1N1) virus. *Virology* **160**, 31–37.
17. Schild, G.C., Oxford, J.S., de Jong, J.C. & Webster, R.G. (1983). Evidence for host-cell selection of influenza virus antigenic variants. *Nature* **303**, 706–709.
18. Kodihalli, S., Justewicz, D.M., Gubareva, L.V. & Webster, R.G. (1995). Selection of a single amino acid substitution in the hemagglutinin molecule by chicken eggs can render Influenza A virus (H3) candidate vaccine ineffective. *J. Virol.* **69**, 4888–4897.
19. Meyerhans, A., *et al.*, & Wain-Hobson, S. (1989). Temporal fluctuations in HIV quasi species in vivo are not reflected by sequential isolations. *Cell* **58**, 901–910.
20. Diez, J., *et al.*, & Domingo, E. (1990). Unique amino acid substitutions in the capsid proteins of foot-and-mouth disease virus from a persistent infection in cell culture. *J. Virol.* **64**, 5519–5528.
21. Mason, P.W., Rieder, E. & Baxt, B. (1994). RGD sequence of foot-and-mouth disease virus is essential for infecting cells via the natural receptor but can be bypassed by an antibody-dependent enhancement pathway. *Proc. Natl. Acad. Sci. USA* **91**, 1932–1936.
22. Yewdell, J.W., Caton, A.J. & Gerhard, W. (1986). Selection of influenza A virus adsorptive mutants by growth in the presence of a mixture of monoclonal antihemagglutinin antibodies. *J. Virol.* **57**, 623–628.
23. Temoltzin-Palacios, F. & Thomas, D.B. (1994). Modulation of immunodominant sites in influenza hemagglutinin compromise antigenic variation and select receptor-binding variant viruses. *J. Exp. Med.* **179**, 1719–1724.
24. Fox, G., Parry, N.R., Barnett, P.V., McGinn, B., Rowlands, D. & Brown, F. (1989). The cell attachment site on foot-and-mouth disease virus includes the amino acid sequence RGD (arginine–glycine–aspartic acid). *J. Gen. Virol.* **70**, 625–637.
25. Baxt, B. & Becker, Y. (1990). The effect of peptides containing the arginine–glycine–aspartic acid sequence on the adsorption of foot-and-mouth disease virus to tissue culture cells. *Virus Genes* **4**, 73–83.
26. Saiz, J.C., Gonzalez, M.J., Borca, M.V., Sobrino, F. & Moore, D.M. (1991). Identification of neutralizing antigenic sites on VP1 and VP2 of type A5 foot-and-mouth disease virus, defined by neutralization-resistant variants. *J. Virol.* **65**, 2518–2524.
27. Thomas, A.A.M., Woortmeijer, R.J., Puijk, W. & Barteling, S.J. (1988). Antigenic sites on foot-and-mouth disease virus type A10. *J. Virol.* **62**, 2782–2789.
28. Kitson, J.D.A., McCahon, D. & Belsham, G.J. (1990). Sequence analysis of monoclonal antibody resistant mutants of type O foot and mouth disease virus: evidence for the involvement of three surface exposed capsid proteins in four antigenic sites. *Virology* **179**, 26–34.
29. Baxt, B., Vakharia, V., Moore, D.M., Franke, A.J. & Morgan, D.O. (1989). Analysis of neutralizing antigenic sites in the surface of type A12 foot-and-mouth disease virus. *J. Virol.* **63**, 2143–2151.
30. Rweyemamu, M.M., Ouldridge, E.J., Head, M. & Purse, F. (1984). Evaluation of the antigenic variation within type A foot and mouth disease virus isolates from Asia. *J. Biol. Stand.* **12**, 191–194.
31. Bolwell, C., Parry, N.R. & Rowlands, D.J. (1992). Comparison between *in vitro* neutralization titres and *in vivo* protection against homologous and heterologous challenge induced by vaccines prepared from two serologically distinct variants of foot-and-mouth disease virus, serotype A22. *J. Gen. Virol.* **73**, 727–731.
32. Palmenberg, A.C. (1989). Sequence alignments of picornaviral capsid proteins, In *Molecular Aspects of Picornavirus Infection and Detection*, (Semler, B.L. & Ehrenfeld, E., eds), pp. 211–241, American Society for Microbiology, Washington.
33. Logan, D., *et al.*, & Fry, E. (1993). Structure of a major immunogenic site on foot-and-mouth disease virus. *Nature* **362**, 566–568.
34. Bittle, J.L., *et al.*, & Brown, F. (1982). Protection against foot-and-mouth disease virus by immunization with a chemically synthesized peptide predicted from the viral nucleotide sequence. *Nature* **298**, 30–33.
35. DiMarchi, R., Brooke, G., Gale, C., Cracknell, V., Doel, T. & Mowat, N. (1986). Protection of cattle against foot-and-mouth disease virus by a synthetic peptide. *Science* **232**, 639–641.
36. Stromaier, K., Franze, R. & Adamm, K.-H. (1982). Location and characterization of the antigenic portion of the FMDV immunising protein. *J. Gen. Virol.* **59**, 295–306.
37. Verdagauer, N., Mateu, M.G., Andreu, D., Giralt, E., Domingo, E. & Fita, I. (1995). Structure of the major antigenic loop of foot-and-mouth disease virus complexed with a neutralizing antibody: direct involvement of the Arg–Gly–Asp motif in the interaction. *EMBO J.* **14**, 1690–1696.
38. Parry, N. R., *et al.*, & Stuart, D. (1990). Structural and serological evidence for a novel mechanism of antigenic variation in foot-and-mouth disease virus. *Nature* **347**, 569–572.
39. Bolwell, C., Clarke, B.E., Parry, N.R., Ouldridge, E., Brown, F. & Rowlands, D.J. (1989). Epitope mapping of foot-and-mouth disease virus with neutralizing monoclonal antibodies. *J. Gen. Virol.* **70**, 59–68.
40. Hwang, S.S., Boyle, T.J., Lyerly, H.K. & Cullen, B.R. (1991). Identification of the envelope V3 loop as the primary determinant of cell tropism in HIV-1. *Science* **253**, 71–74.
41. Milich, L., Margolin, B. & Swanstrom, R. (1993). V3 Loop of the Human immunodeficiency virus type 1 Env protein: interpreting sequence variability. *J. Virol.* **67**, 5623–5634.
42. Shioda, T., *et al.*, & Nagai, Y. (1994). A naturally occurring single basic amino acid substitution in the V3 region of the human immunodeficiency virus type 1 Env protein alters the cellular host range and antigenic structure of the virus. *J. Virol.* **68**, 7689–7696.
43. Hattori, T., Koito, A., Takatsuki, K., Kido, H. & Katunuma, N. (1989). Involvement of tryptase-related cellular protease(s) in human immunodeficiency virus type 1 infection. *FEBS Lett.* **248**, 48–52.
44. Kido, H., Fukutomi, A. & Katunuma, N. (1990). A novel membrane-bound serine esterase in muman $T4^+$ lymphocytes immunologically reactive with antibody inhibiting syncytia induced by HIV-1. *J. Biol. Chem.* **265**, 21979–21985.
45. Stephens, P.E., Clements, G. & Yarranton, G.T. (1990). A chink in HIV's armour? *Nature* **343**, 219.
46. Javaherian, K., *et al.*, & Matthews, T.J. (1989). Principal neutralizing domain of the human immunodeficiency virus type 1 envelope protein. *Proc. Natl. Acad. Sci. USA* **86**, 6768–6772.
47. Palker, T.J., *et al.*, & Haynes, B.F. (1988). Type-specific neutralization of the human immunodeficiency virus with antibodies to env-encoded synthetic peptides. *Proc. Natl. Acad. Sci. USA* **85**, 1932–1936.
48. Pfaff, E., Mussgay, M., Bohm, H.O., Schulz, G.E. & Schaller, H. (1982). Antibodies against a preselected peptide recognize and neutralise foot-and-mouth disease virus. *EMBO J.* **1**, 869–874.
49. Rieder, E., Baxt, B. & Mason, P.W. (1994). Animal-derived antigenic variants of foot-and-mouth disease virus type A12 have low affinity for cells in culture. *J. Virol.* **68**, 5296–5299.
50. Curry, S., *et al.*, & Stuart, D. (1992). Crystallization and preliminary X-ray analysis of three serotypes of foot-and-mouth disease virus. *J. Mol. Biol.* **228**, 1263–1268.
51. Harlos, K. (1992). Microbridges for sitting drop crystallizations. *J. Appl. Cryst.* **25**, 536–538.
52. Stura, E.A. & Wilson, I.A. (1990). Analytical and production seeding techniques. *Methods* **1**, 38–49.
53. Fry, E., Acharya, R. & Stuart, D. (1993). Methods used in the structure determination of foot-and-mouth disease virus. *Acta Cryst. A* **49**, 45–55.
54. Collaborative Computational Project, Number 4. (1994). The CCP4 Suite: programs for protein crystallography. *Acta Cryst. D* **50**, 760–763.
55. Brünger, A.T. (1992). *X-PLOR Version 3.0.* Yale University, Newhaven, CT.
56. Jones, T.A. (1978). Interactive computer graphics: FRODO. *Methods Enzymol.* **115**, 157–171.
57. Engh, R.A. & Huber, R. (1991). Accurate bond and angle parameters for X-ray protein-structure refinement. *Acta Cryst. A* **47**, 392–400.
58. Jones, T.A., Zou, J.Y., Cowan, S.W. & Kjeldgaard, M. (1991). Improved methods for building protein models in electron density maps and the location of errors in these maps. *Acta Cryst. A* **47**, 110–119.